S1–S34

Electronic Supporting Information

Phenoxazinyl Zn(II) diradical complex formed via redox-driven cyclization of a 2-aminophenol-based N_3O ligand. Isolation of modified N_3 ligand radical and its Ni(II) complex

Narottam Mukhopadhyay, Arunava Sengupta, Francesc Lloret and Rabindranath Mukherjee*

Contents

Experimental details

Solvents and reagents

All the reagents were obtained from commercial sources and used as received. Solvents were dried/purified according to reported procedures.[1] Synthesis of precursor metal salt $Zn(ClO_4)_2 \cdot 6H_2O$ and TBAP (tetrabutylammonium perchlorate) were prepared following reported procedures.[2]

Syntheses

Synthesis of *N*-(2-((3,5-Di-*tert*-butyl-2-hydroxyphenyl)amino)phenyl)picolinamide, H_3L^1

The synthesis of the ligand H_3L^1 was done by following our previous report.[3] The ligand was purified by column chromatography (10% ethyl acetate in *n*-hexane), and an excellent yield of 95% was obtained.

^{1}H NMR (500 MHz; $CDCl_3$ δ (ppm) 9.99 (s, 1H; –CONH), 8.64 (d, *J* = 5.5 Hz, 1H; Py), 8.32 (d, *J* = 10 Hz, 1H), 7.89 (t, *J* = 9.5 Hz, 1H), 7.51 (t, *J* = 6.5 Hz, 1H), 7.43 (d, *J* = 9.5 Hz, 1H), 7.21 (d, *J* = 2.5 Hz, 1H), 7.10 (t, *J* = 9.5 Hz, 1H), 7.06 (d, *J* = 2.5 Hz, 1H), 6.90 (t, *J* = 9.5 Hz, 1H), 6.77 (s, 1H; NH), 6.63 (d, *J* = 10.5 Hz, 1H), 5.69 (s, 1H; OH), 1.44 (s, 9H; *tert*–butyl), 1.28 (s, 9H; *tert*–butyl).

Synthesis of complex $[Zn(L^{1*})_2]$ (1)

To a solution of H_3L^1 (0.1 g, 0.24 mmol) in CH_3CN (5 mL), Et_3N (0.073 g, 0.72 mmol) was added and stirred for 15 min. Then solid $Zn(ClO_4)_2 \cdot 6H_2O$ (0.096 g, 0.24 mmol), dissolved in CH_3CN (3 mL), was added dropwise to stirring red deprotonated ligand solution dropwise, and the resulting mixture was refluxed for 6 h. The colour of the solution changed from red to brownish-red to dark brown. The resulting mixture was cooled, reduced to one-fourth of its original volume under reduced pressure, and kept in a refrigerator for 1 h. The dark brown precipitate that separated was collected by filtration, washed with cold CH_3CN and CH_3OH, and dried *in vacuo*. Yield: 0.12 g (~90% with respect to H_3L^1).

Anal. Calcd. (%) for $C_{52}H_{54}N_6ZnO_4$ (fw = 892.42): C, 69.99; H, 6.10; N, 9.42. Found: C, 69.89; H, 6.18; N, 9.43. Suitable single crystals for X-ray diffraction studies were obtained by slowly evaporating the solution mixture (CH_2Cl_2-CH_3OH (4:1, v/v)) of **1**.

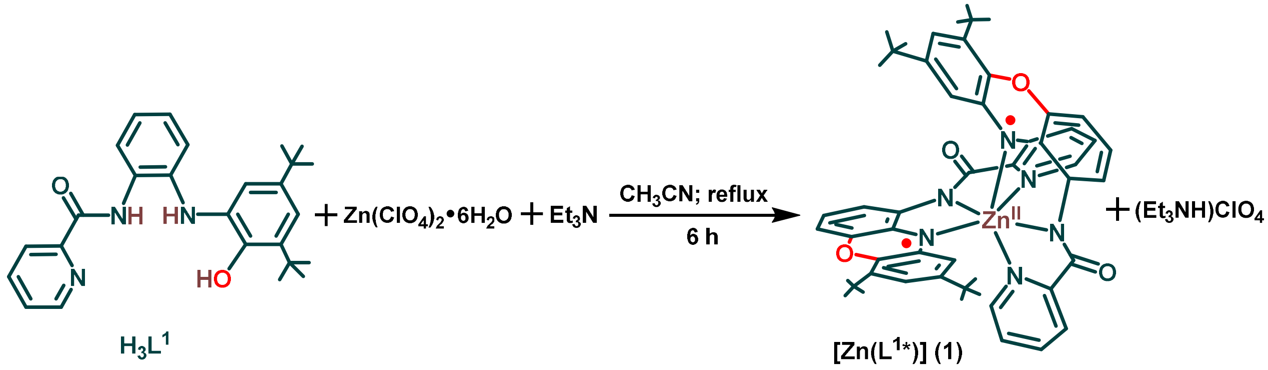

Synthesis of **1**.

Note: Attempts were made to synthesize similar diradical phenoxazinylate complexes using d^0 metal ions, Mg^{2+} and Ca^{2+}. In both cases, the above-mentioned synthetic procedure (Synthesis of **1)** was followed with $Ca(ClO_4)_2$•xH_2O or $MgCl_2$ as metal salts. However, all our attempts to isolate a particular species resulted in a mixture of products. We have so far been unsuccessful in isolating a clean species. Moreover, ESI-MS (+ve-ion mode) analysis of the reaction mixture did not reveal peaks corresponding to a clean complexation reaction product. Instead, peaks corresponding to the modified ligand (L^1*) and its homo-coupled derivatives are detected.[4] The poor complexation reaction may be attributed to the smaller size of the corresponding M^{2+} (Mg, Ca) ions. Nevertheless, the interaction between the ligand and the M^{2+} ions facilitates the preorganization of deprotonated ligand $(L^1)^{3-}$, aiding in the successive formation of the phenoxazinylate core through intramolecular oxidative cyclization. Corresponding ESI-MS reports are in Figs. S14 and S15, respectively.

Demetalation of 1 (Isolation of HL^{1*}•$HClO_4$)

0.1 g of complex **1** was dissolved in 5 ml of CH_2Cl_2. A few drops of perchloric acid (70%) were added to this brown complex solution till it turned purple. The resulting mixture was stirred for 1 h at 298 K. The mixture was concentrated under reduced pressure and kept in a refrigerator for 30 min after adding 10 ml of diethyl ether. A deep purple precipitate that separated was collected by filtration, washed with cold dry CH_2Cl_2, dry diethyl ether, and dry *n*-pentane and dried *in vacuo*. The crude was isolated with an excellent yield of 95% (with respect to complex **1**).

Anal. Calcd. (%) for $C_{26}H_{29}N_3O_6Cl$ (fw = 514.98): C, 69.64; H, 5.68; N, 8.16. Found: C, 69.58; H, 5.79; N, 8.12. IR (KBr, cm^{-1}, selected peak): *ν*(ClO_4) 1089, 626.

Note: The purple colour of the compound solution is very stable in dry solvents (CH_3CN, CH_2Cl_2 etc) or in acetic acid, but the presence of water or an increase in the pH over 7 leads to a change in solution colour to green.

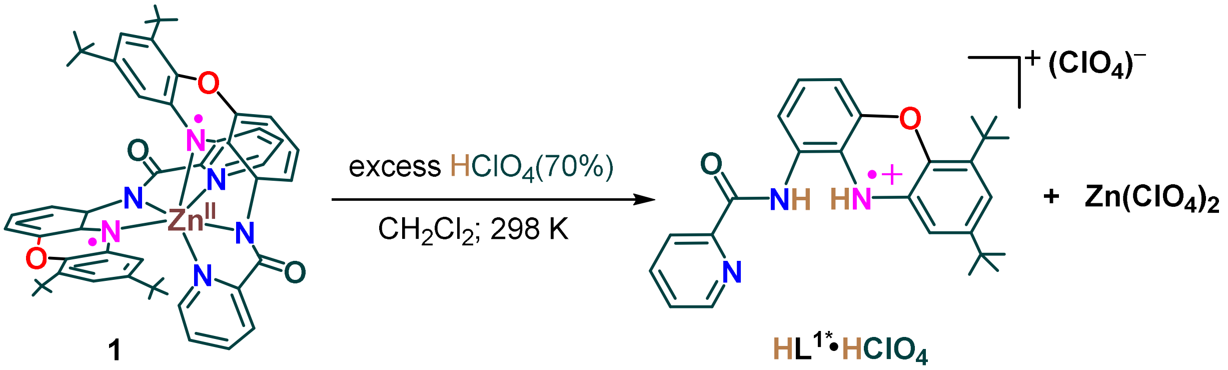

Demetallation of **1**.

Synthesis of complex [Ni(L^{1*})$_2$] (2)

To a magnetically stirred solution of $HL^{1*}\bullet HClO_4$ (0.1 g, 0.19 mmol) in CH_3CN, Et_3N (0.04 g, 0.39 mmol) was added. The purple solution immediately turned green and was allowed to stir for another 5 min. Solid $Ni(OAc)_2\bullet 4H_2O$ (0.05 g, 0.20 mmol) was added aerobically, and the resulting mixture was stirred continuously at 295 K for 4 h. The colour of the solution changed from greenish-brown to yellowish-brown. The resulting mixture was concentrated under reduced pressure and kept in a refrigerator for 1 h. A deep brown precipitate was separated upon filtration, washed with cold CH_3CN and CH_3OH, and dried *in vacuo*. The crude was isolated in an excellent yield of 90%.

Anal. Calcd. (%) for $C_{52}H_{54}N_6NiO_4$ (fw = 885.73): C, 70.51; H, 6.15; N, 9.49. Found: C, 70.54; H, 6.11; N, 9.44. Suitable single crystals for X-ray diffraction studies were obtained by layering *n*-hexane over a CH_2Cl_2 solution of complex **2**.

Physical measurements

Elemental analyses were obtained using a Perkin Elmer CHN Analyzer (2400 series). Spectroscopic measurements were made using the following instruments: Absorption spectra were recorded using an Agilent diode array Cary 8454 spectrophotometer (200−1100 nm); IR

(KBr, 4000–400 cm^{-1}), Bruker Vector 22. ^{1}H NMR spectra were recorded on a Bruker 500 (500 MHz) spectrometer. Chemical shifts are reported in ppm referenced to $CDCl_3$. HRMS spectra were recorded with Waters Xevo G2-XS QToF and Bruker maXis impact. X-Band EPR spectra were recorded using a Bruker EMX 1444 EPR spectrometer (fitted with a quartz Dewar for 100 K measurements), operating at ~ 9.4 GHz. The EPR spectra were calibrated with diphenylpicrylhydrazyl, DPPH (g = 2.0037). Spectral acquisitions were made using the Bruker WINEPR software and simulated using the Bruker SIMFONIA software.

Cyclic voltammetric (CV) experiments were performed at 298 K using CH Instruments, Electrochemical Analyzer/Workstation Model 600B Series. The cell contained a platinum (CHI101) working electrode, a platinum wire auxiliary electrode, and a saturated calomel electrode (SCE) as a reference electrode.[2,5] The solutions were ~1.0 mM in complex and 0.1 M in supporting electrolyte TBAP. Under our experimental conditions, the $E_{1/2}$ and peak-to-peak separation (ΔE_p) values for $[Fe(\eta^5\text{-}C_5H_5)_2]^+$ / $[Fe(\eta^5\text{-}C_5H_5)_2]$ (Fc^+ / Fc) couple are 0.45 V *vs.* SCE and 100 mV in CH_2Cl_2.[4] All potentials are reported with respect to (Fc^+ / Fc) couple. Both redox processes are chemically reversible (ratio of cathodic and anodic peak current) and electrochemically reversible[11] (based on Fc^+/Fc couple under identical experimental conditions), except the second reduction which is quasireversible in nature.[5]

Temperature-dependent magnetic measurement on complex **1** was carried out using a Quantum Design SQUID magnetometer (València, Spain) at 0.01 T for $T < 50$ K to avoid saturation effects and 0.1 T for $T > 50$ K. Effective magnetic moment is calculated from $\mu_{\text{eff}} = 2.828[\chi_M T]^{1/2}$, where χ_M is the corrected molar susceptibility. Diamagnetic corrections were applied to the susceptibility data.[6] Solution-state magnetic susceptibilities were obtained by the NMR method of Evans[7] in CH_2Cl_2 with a Bruker 500 spectrometer and used the paramagnetic shift of the methyl protons of TMS as the measured NMR parameter. Solvent susceptibility data was taken from the literature value.[6] The magnetic susceptibility data can be satisfactorily fitted using a modified version of the Bleaney-Bowers equation (eq 1).[6,8]

$$\chi = \frac{2Ng^2\beta^2}{kT\left[3+e^{-J/kT}\right]}(1-\rho) + \frac{Ng^2\beta^2}{2kT}\,\rho \qquad (1)$$

Crystallographic data collection

Single crystals of suitable dimensions for **1**, **PhZ**•0.75CH_2Cl_2, and **2** were used for data collection. Diffraction intensities were collected with a Bruker SMART APEX-II CCD diffractometer with graphite-monochromated Mo-K_α (λ = 0.71073 Å) radiation at 100(2) K at 100(2) K. The data were corrected for absorption. The 'Bruker SAINT V8.38A' was used for data reduction. Data were also corrected for Lorentz and polarisation effects; multi-scan absorption corrections (SADABS-2016/2) were applied. The structures were solved with SHELXT and refined with the SHELXL–2018/3 package,[9a] incorporated into the Olex2 1.5-alpha crystallographic collective package.[9a-c] The position of hydrogen atoms was calculated by assuming ideal geometries and included in the last refinement cycle. All non-hydrogen atoms were refined with anisotropic thermal parameters by full-matrix least-squares minimization procedures on F^2. The OMIT command was used in all three data sets to remove the insufficient quality data at low-angle. In the case of **PhZ**•0.75CH_2Cl_2 the collected data set is of very poor quality. Complete solving is not possible with the current data, but the best possible structure is given here. Non-merohedral twinning is detected, and a corresponding HLK5 file has been generated using the PLATON function. BASF 0.29802 factor has been introduced in the refinement cycle. To check the ADPs (anisotropic displacement parameters), the SIMU 0.02 0.02 1.7 restraint was applied to all non-H atoms, ISOR and SADI restraints were applied on several tert-butyl carbon atoms to model. The crystal's unit cell depicts eight **PhZ** units (eight $[H_2L^{1*}]^+$ and eight SbF_6^- ions) and six CH_2Cl_2 solvent molecules. Thus, the reported Z value of the crystal is 8 and Z' is 4. Unassigned high residual density (+3.010 eÅ^{-3}) Q-peak is present. Unfortunately, we could not grow single crystals of **PhZ** that were any better than the one used for the present study, as they were the best we could have. The details of data collection and structure refinement are in Table S1.

Computational methodologies

All DFT calculations were performed using Gaussian 09 program.[10] Optimizations were carried out employing X-ray coordinates with a B3LYP functional.[11] Triple-ζ quality basis-set (TZVP)[12] was used for Zn, N, and O, while SVP basis-set[13] was used for C and H. For the spin-polarized broken-symmetry (BS) solution, the broken-symmetry formalism was introduced by Noodleman.[14] For two-centre electron system, the high spin states ($M_s = 1$) were calculated. Then these high spin wave functions were used as initial guesses, along with the additional keyword “Guess=Mix” for the geometry optimization of BS ($M_s = 0$) surface for final atomic coordinates. For the two-centre electron system, the magnetic-exchange coupling was modelled with the well-known Heisenberg–Dirac–van Vleck Hamiltonian:

$\hat{H}_{\mathrm{HDVV}} = -2J_{12}\cdot\hat{S}_1\cdot\hat{S}_2$ (2)

Based on the above Hamiltonian (eq 2), three well-known approaches are reported in the literature[13] to calculate the magnetic-exchange coupling value $2J$. The approach proposed by Noodleman is eq (3).[14,15]

$J = -(E_{\mathrm{HS}} - E_{\mathrm{BS}})/S^2_{\mathrm{max}}$ (3)

where E_{HS} and E_{BS} are the energies of the high-spin (HS; $M_{\mathrm{S}} = S_1 + S_2$) and BS determinants ($M_{\mathrm{S}} = |S_1 - S_2|$)

The second one proposed by Bencini et al. (eq 4)[16]

$J = -(E_{HS} - E_{BS}) / [S_{\mathrm{max}}(S_{\mathrm{max}} + 1)]$ (4)

Third-one is proposed by Yamaguchi et al. (eq 5)[17]

$J = -(E_{HS} - E_{BS})/(\langle S^2\rangle_{\mathrm{HS}} - \langle S^2\rangle_{\mathrm{BS}})$ (5)

Yamaguchi approach explicitly uses the expectation values of the square of the spin ($\langle S^2\rangle$), provided by the output of the unrestricted DFT calculations. It has nicely been explained by Neese[15] stating that Yamaguchi approach is valid for a whole range of coupling strengths (from weak- to strong-exchange interaction), and it reduces to the Noodleman equation in the weak-coupling limit. Here, the J value has been calculated with the help of Yamaguchi’s expression.

TD-DFT calculations employed the B3LYP functional and the polarizable continuum model, CPCM (CH_2Cl_2 as solvent).[18] In the TD-DFT calculations, 40 states have been included. TD-DFT-derived electronic spectra were plotted using GaussSum.[19] Corresponding orbitals were made using the Chemcraft[20] Visualization program.

References

1 (*a*) A. Mukherjee and R. Mukherjee, *Indian J. Chem.*, 2011, **50A**, 484; (*b*) A. Rajput, A. K. Sharma, S. K. Barman, D. Koley, M. Steinert and R. Mukherjee, *Inorg. Chem.*, 2014, **53**, 36; (*c*) A. Saha, A. Rajput, P. Gupta and R. Mukherjee, *Dalton Trans.*, 2020, **49**, 15355.

2 M. Ray, S. Mukerjee and R. Mukherjee, *J. Chem. Soc., Dalton Trans.*, 1990, 3635.

3 N. Mukhopadhyay, A. Sengupta, A. K. Vijay, F. Lloret and R. Mukherjee, *Dalton Trans.*, 2022, **51**, 9017.

4 (*a*) T. J. Kemp, P. Moore, and G. R. Quick, *J. Chem. Soc., Perkin Trans.* 1980, **2**, 291; (*b*) H. Roseboom and J. H. Perrin, *J. Pharmacol. Sci.*, 1977, **66**, 1395.

5 R. Mukherjee, C. P. Rao and R. H. Holm, *Inorg. Chem.*, 1986, **25***,* 2979.

6 C. J. O'Connor, *Prog. Inorg. Chem.*, 1982, **29**, 203.

7 (*a*) D. F. Evans, *J. Chem. Soc.*, 1959, 2003; (*b*) W. Gerger, U. Mayer and V. Gutmann, *Monatsh. Chem.*, 1977, **108**, 417.

8 O. Kahn, *Molecular Magnetism*, VCH publisher, 1993.

9 (*a*) O. V. Dolomanov, L. J. Bourhis, R. J. Gildea, J. A. K. Howard and H. Puschmann, *J. Appl. Cryst.*, 2009, **42**, 339; (*b*) G. M. Sheldrick, *Acta Cryst.*, 2015, **A71**, 3; (*c*) G. M. Sheldrick, *Acta Cryst.*, 2015, **C71**, 3.

10 M. J. Frisch, G. W. Trucks, H. B. Schlegel, G. E. Scuseria, M. A. Robb, J. R. Cheeseman, G. Scalmani, V. Barone, B. Mennucci, G. A. Petersson, H. Nakatsuji, M. Caricato, X. Li, H. P. Hratchian, A. F. Izmaylov, J. Bloino, G. Zheng, J. L. Sonnenberg, M. Hada, M. Ehara, K. Toyota, R. Fukuda, J. Hasegawa, M. Ishida, T. Nakajima, Y. Honda, O. Kitao, H. Nakai, T. Vreven, J. A. Montgomery Jr., J. E. Peralta, F. Ogliaro, M. Bearpark, J. J. Heyd, E. Brothers, K. N. Kudin, V. N. Staroverov, R. Kobayashi, J. Normand, K. Raghavachari, A. Rendell, J. C. Burant, S. S. Iyengar, J. Tomasi, M. Cossi, N. Rega, N. J. Millam, M. Klene, J. E. Knox, J. B. Cross, V. Bakken, C. Adamo, J. Jaramillo, R. Gomperts, R. E. Stratmann, O. Yazyev, A. J. Austin, R. Cammi, C. Pomelli, J. W. Ochterski, R. L. Martin, K. Morokuma, V. G. Zakrzewski, G. A. Voth, P. Salvador, J. J. Dannenberg, S. Dapprich, A. D. Daniels, Ö. Farkas, J. B. Foresman, J. V. Ortiz, J. Cioslowski and D. J. Fox, *Gaussian 09, revision C.01, Gaussian, Inc. Wallingford, CT* 2010.

11 (*a*) A. D. Becke and J. Chem. Phys., 1993, **98**, 5648; (*b*) C. Lee, W. Yang and R. G. Parr, *Phys. Rev. B: Condens. Matter Mater. Phys.*, 1988, **37**, 785; (*c*) P. J. Stevens, F. J. Devlin, C. F. Chabalowski and M. J. Frisch, *J. Phys. Chem.,* 1994, **98**, 11623.

12 A. Schafer, C. Huber and R. Ahlrichs, *J. Chem. Phys.*, 1994, **100**, 5829.

13 A. Schafer, H. Horn and R. Ahlrichs, *J. Chem. Phys.*, 1992, **97**, 2571.

14 (*a*) A. P. Ginsberg, *J. Am. Chem. Soc.*, 1980, **102**, 111; (*b*) L. Noodleman and J. G. Norman Jr., *J. Chem. Phys.*, 1979, **70**, 4903; (*c*) L. Noodleman, *J. Chem. Phys.*, 1981, **74**, 5737; (*d*) L. Noodleman and E. R. Davidson, *Chem. Phys.*, 1986, **109**, 131.

15 (*a*) F. Neese, *J. Phys. Chem. Solids.*, 2004, **65**, 781; (*b*) F. Neese, *Coord. Chem. Rev.*, 2009, **253**, 526; (*c*) C. I. Oprea, P. Panait, F. Cimpoesu, I. Humelnicu, M. Ferbinteanu and M. A. Gîrţu, *Theor. Chem. Acc.*, 2012, **131**, 1249.

16 A. Bencini and D. Gatteschi, *J. Am. Chem. Soc.*, 1986, **108**, 5763.

17 (*a*) K. Yamaguchi, Y. Takahara, T. Fueno, *In Applied Quantum Chemistry; Eds.* V. H. Smith, Jr., H. F. Schaefer III and K. Morokuma, *D. Reidel Publishing Co., Boston, MA, USA*; 1986, 155; (*b*) T. Soda, Y. Kitagawa, T. Onishi, Y. Takano, Y. Shigeta, H. Nagao, Y. Yoshioka and K. Yamaguchi, *Chem. Phys. Lett.*, 2000, **319**, 223.

18 (*a*) V. Barone and M. Cossi, *J. Phys. Chem. A*, 1998, **102**, 1995; (*b*) M. Cossi and V. Barone, *J. Chem. Phys.*, 2001, **115**, 4708; (*c*) M. Cossi, N. Rega, G. Scalmani and V. Barone, *J. Comput. Chem.*, 2003, **24**, 669.

19 N. M. O'Boyle, A. L. Tenderholt and K. M. Langner, *J. Comput. Chem.*, 2008, **29**, 839.

20 http://www.chemcraftprog.com/

21 (a) P. Comba, S. Hausberg and B. Martin, *J. Phys. Chem. A.*, 2009, **113**, 6751; (*b*) M. Atanasov, P. Comba, S. Hausberg and B. Martin, *Coord. Chem. Rev.*, 2009, **253**, 2306.

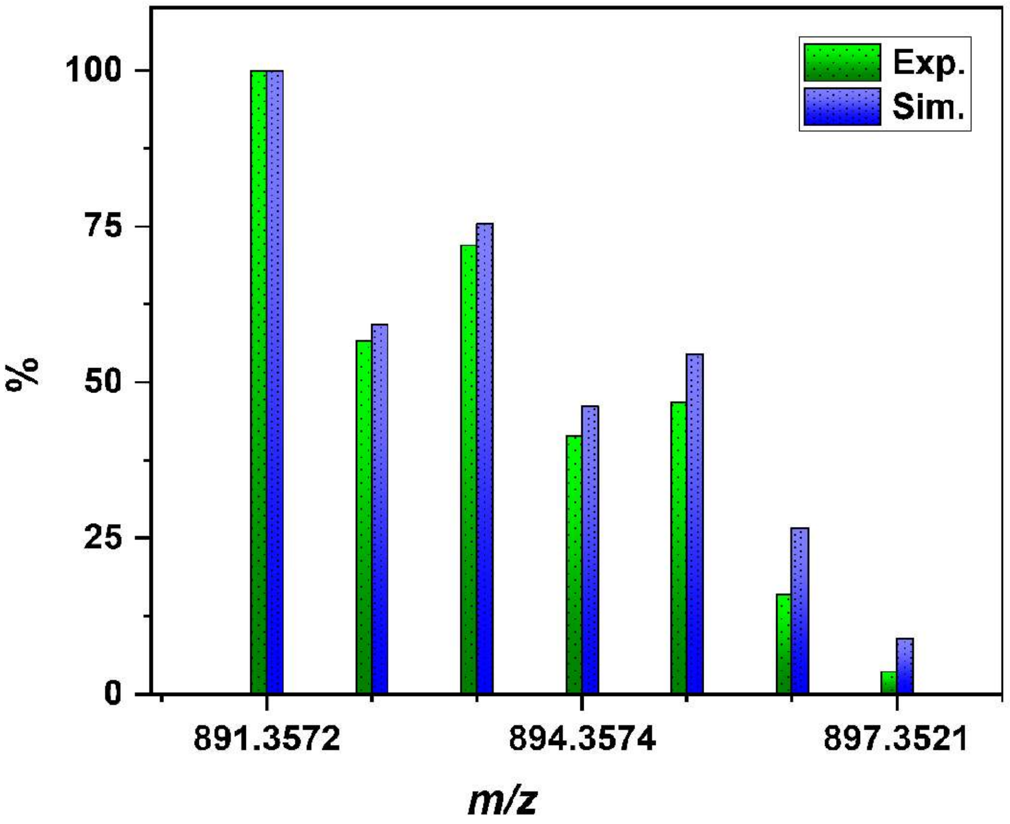

Fig. S1 Positive-Ion ESI-MS spectrum of $[Zn(L^{1*})]$ (**1**): $\{[Zn(L^{1*})_2] + H^+\}$; *m / z* = 891.3572

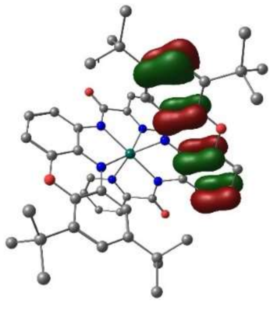

α**–HOMO–7**

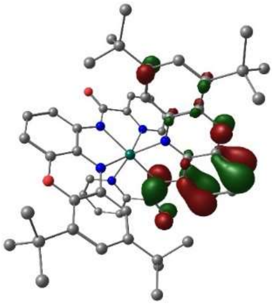

α**–HOMO–1**

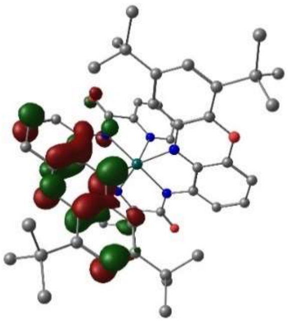

α**–HOMO**

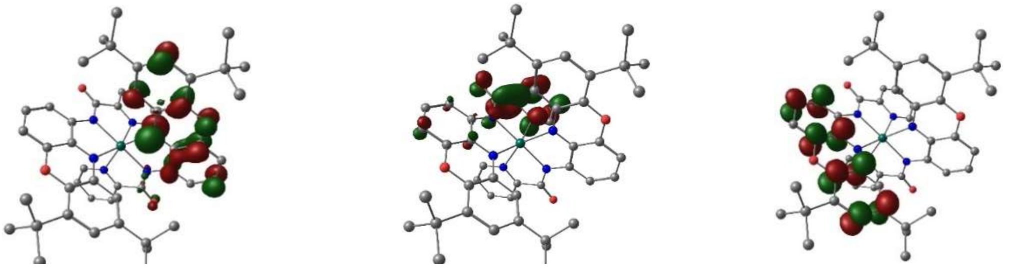

α–LUMO **α–LUMO+1** **α–LUMO+5**

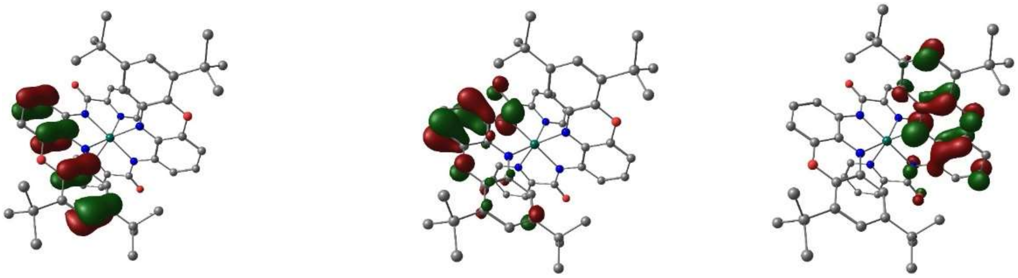

β–HOMO–7 **β–HOMO–1** **β–HOMO**

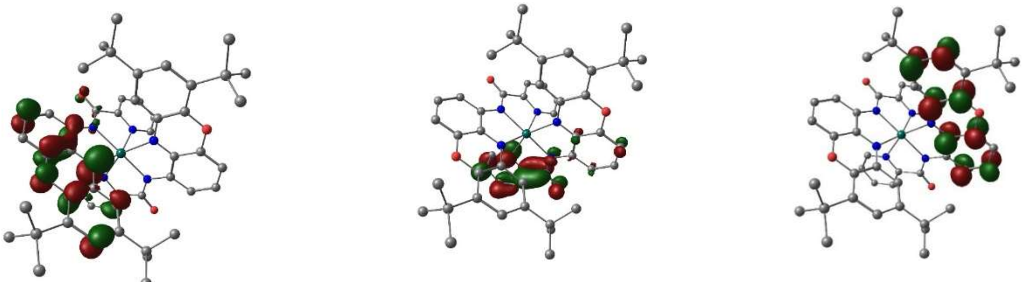

β–LUMO **β–LUMO+1** **β–LUMO+5**

Fig. S2 Representative molecular-orbitals present in TD-DFT transitions of $[\mathrm{Zn}^{\mathrm{II}}\{(\mathrm{L}^{1}*)^{\bullet-}\}_2]$ (**1**) ($M_{\mathrm{S}} = 0$).

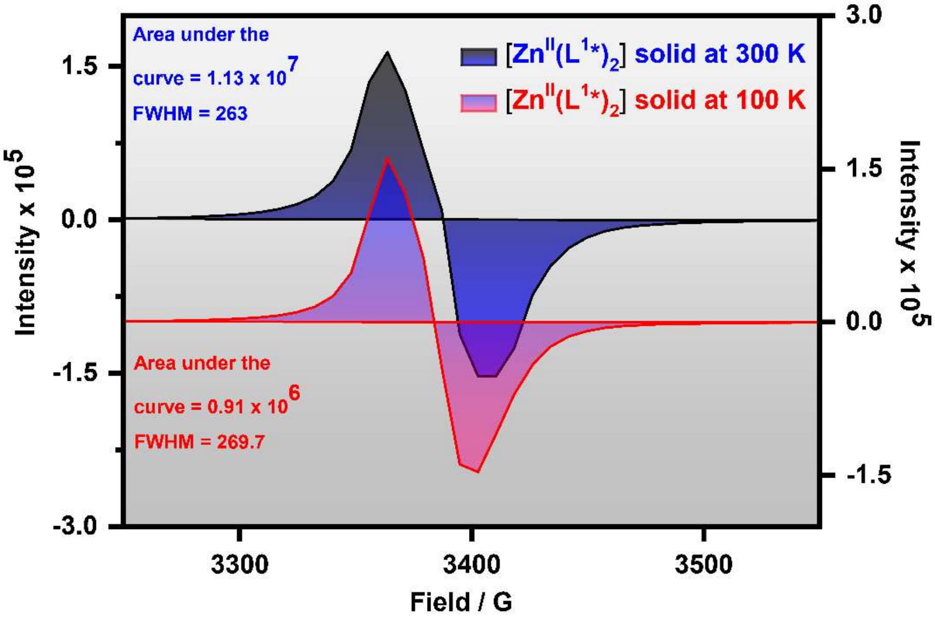

Fig. S3 X-band EPR spectrum (ν = 9.460 GHz, receiver gain = 1 x 10^2, modulation frequency = 100 KHz, modulation amplitude = 10.00 G) for **1** as solid. The upper trace is at 300 K, and the lower trace is at 100 K. The corresponding g_{av} value is 1.995.

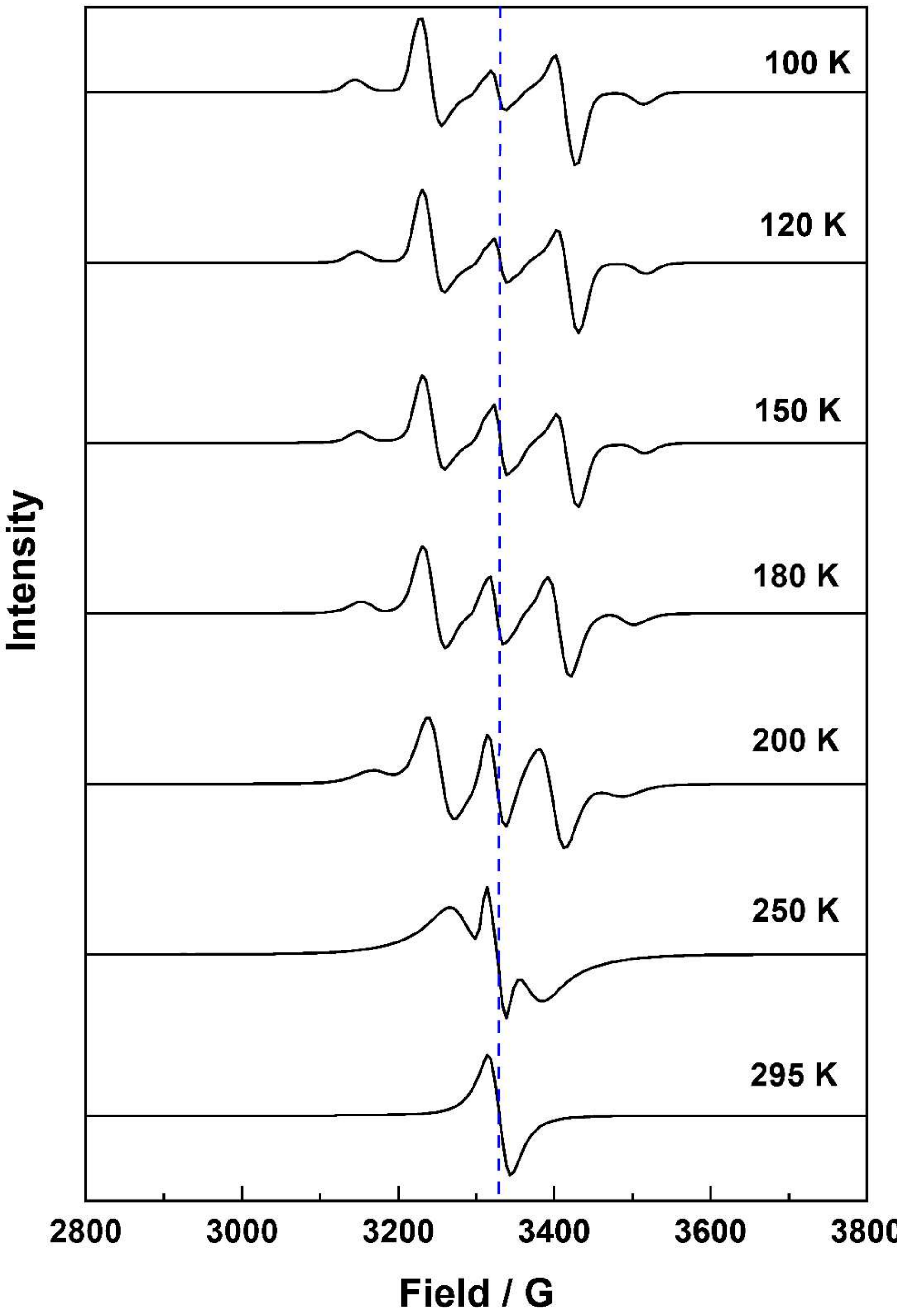

Fig. S4 Variable-temperature (100 – 295 K) X-band (ν = 9.372 GHz, receiver gain = 1 x 10^3, modulation frequency = 100 KHz, modulation amplitude = 10.00 G) EPR spectra of $[Zn^{II}\{(L^1*)^{\bullet-}\}_2]$ (**1**) in CH_2Cl_2-toluene glass (1:1 v/v). Blue marker represents *g* value of 1.998.

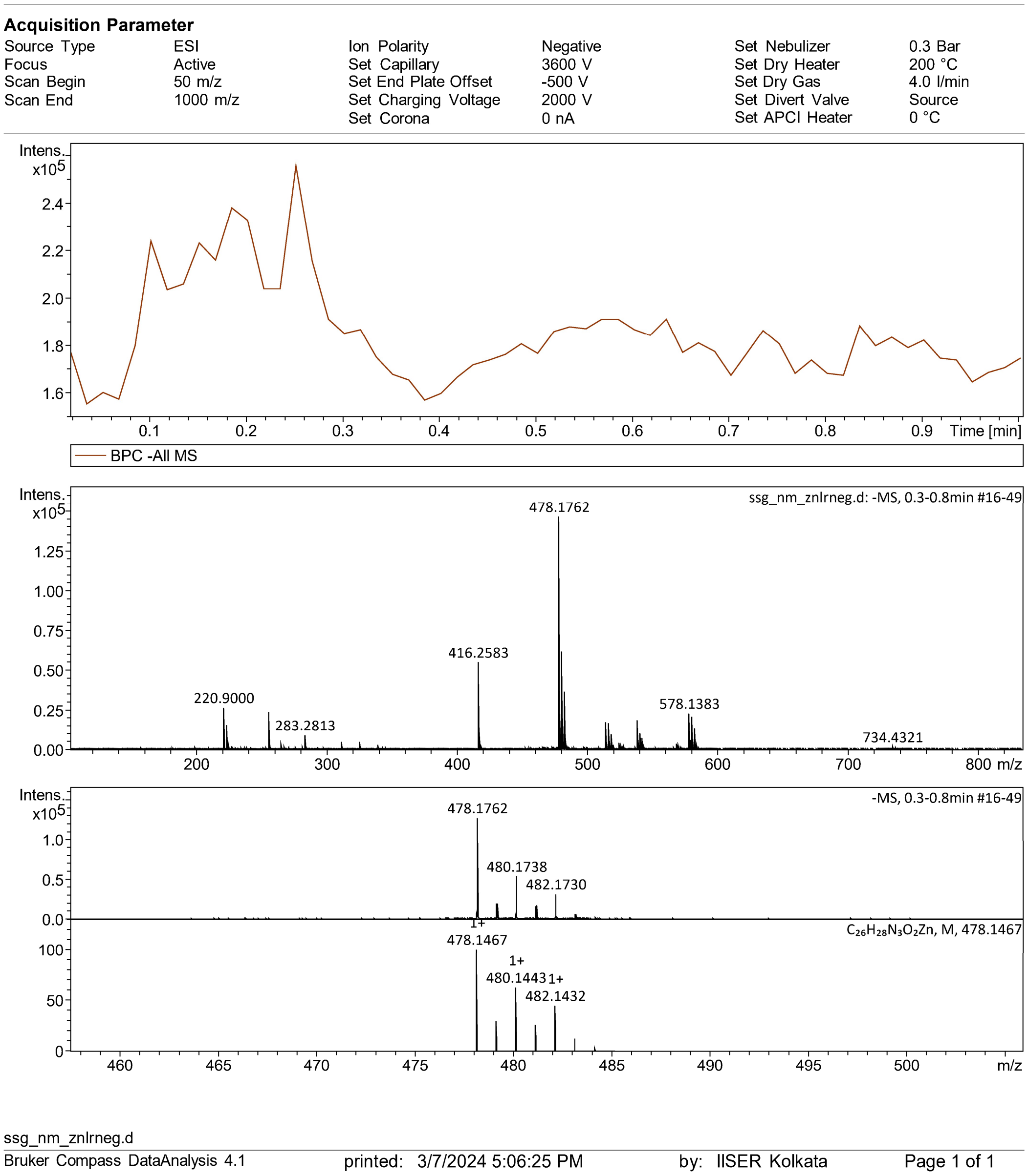

Acquisition Parameter

Source Type	ESI	Ion Polarity	Negative	Set Nebulizer	0.3 Bar
Focus	Active	Set Capillary	3600 V	Set Dry Heater	200 °C
Scan Begin	50 m/z	Set End Plate Offset	-500 V	Set Dry Gas	4.0 l/min
Scan End	1000 m/z	Set Charging Voltage	2000 V	Set Divert Valve	Source
		Set Corona	0 nA	Set APCI Heater	0 °C

ssg_nm_znlrneg.d

Bruker Compass DataAnalysis 4.1 printed: 3/7/2024 5:06:25 PM by: IISER Kolkata Page 1 of 1

Fig. S5 Negative-Ion ESI-MS spectrum of $[Zn^{II}\{(L^1)^{3-}\}]^-$ species: m/z = 478.1467/478.1762 (calcd/found).

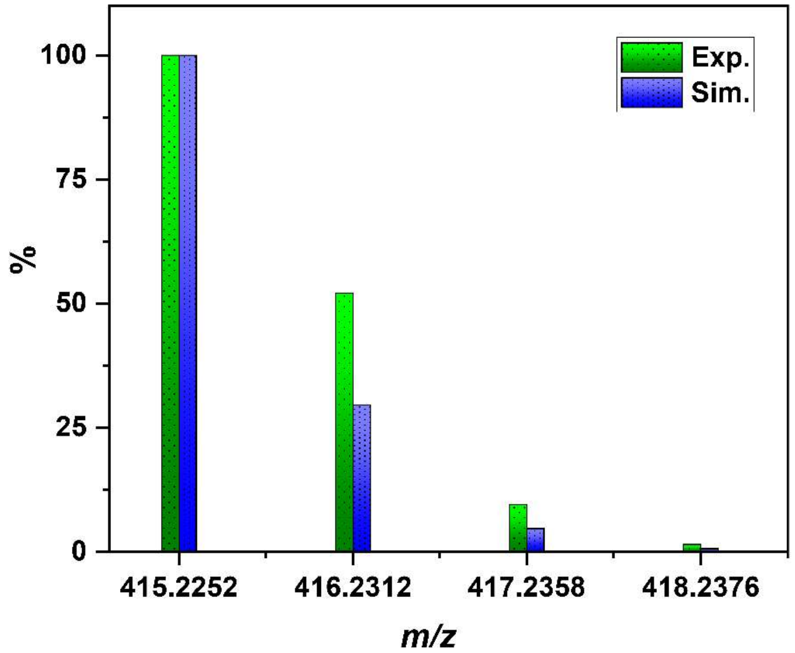

Fig. S6 Positive-Ion ESI-MS spectrum of HL^{1}*•HClO$_4$: {H$_2$L^{1*}}$^+$; *m / z* = 415.2252.

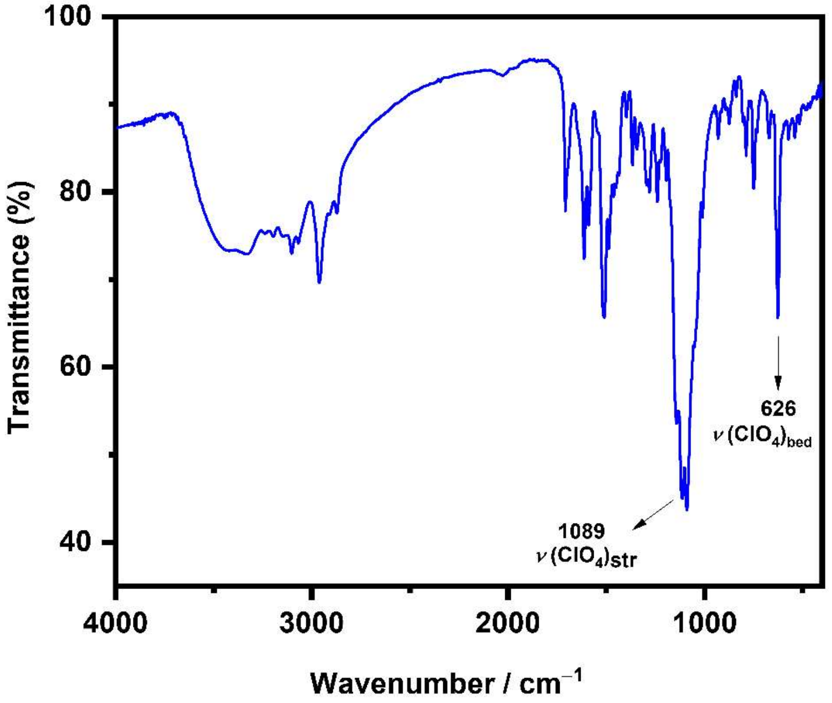

Fig. S7 IR (in KBr) spectrum of HL^{1}*•HClO$_4$.

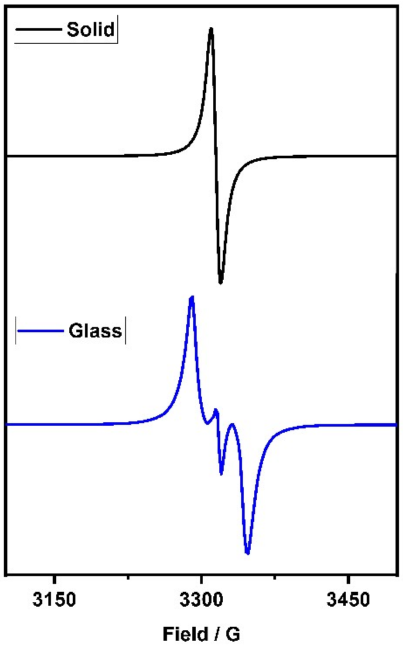

Fig. S8 X-band EPR spectra (ν = 9.410 GHz, receiver gain = 1 x 10^2, modulation frequency = 100 KHz, modulation amplitude = 10.00 G) for HL^{1*}•$HClO_4$ at 100 K. Upper trace: HL^{1*}•$HClO_4$ as solid (g_{iso} = 2.005). Lower trace: HL^{1*}•$HClO_4$ in CH_3CN-toluene glass (3:1 v/v); g_{av} = 2.003.

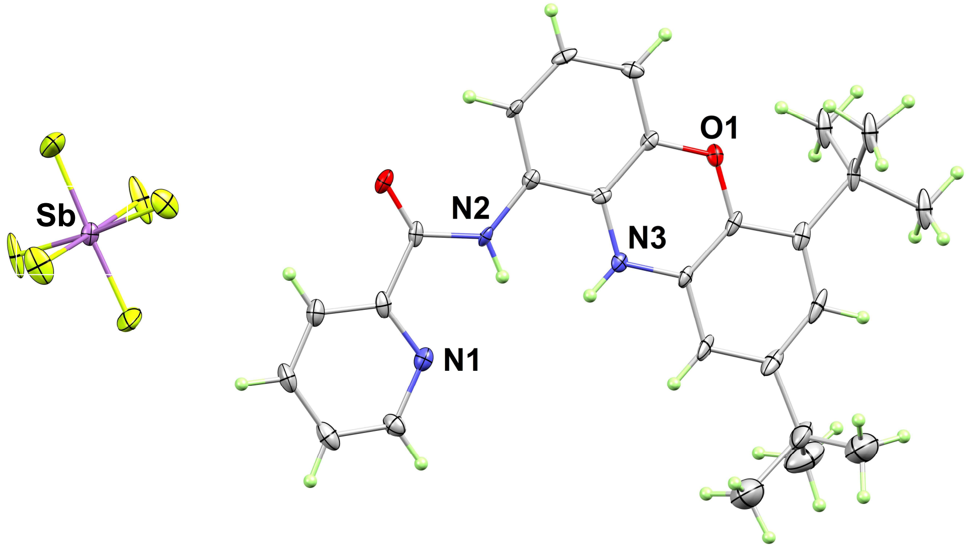

Fig. S9 Perspective view of **PhZ**•0.75CH_2Cl_2 (Phz = [H_2L^{1*}](SbF_6)) with 20% thermal ellipsoid probability. The asymmetric unit contains 4 PhZ and 3 CH_2Cl_2 molecules. Only one PhZ unit is shown, and the solvent molecules are omitted for clarity.

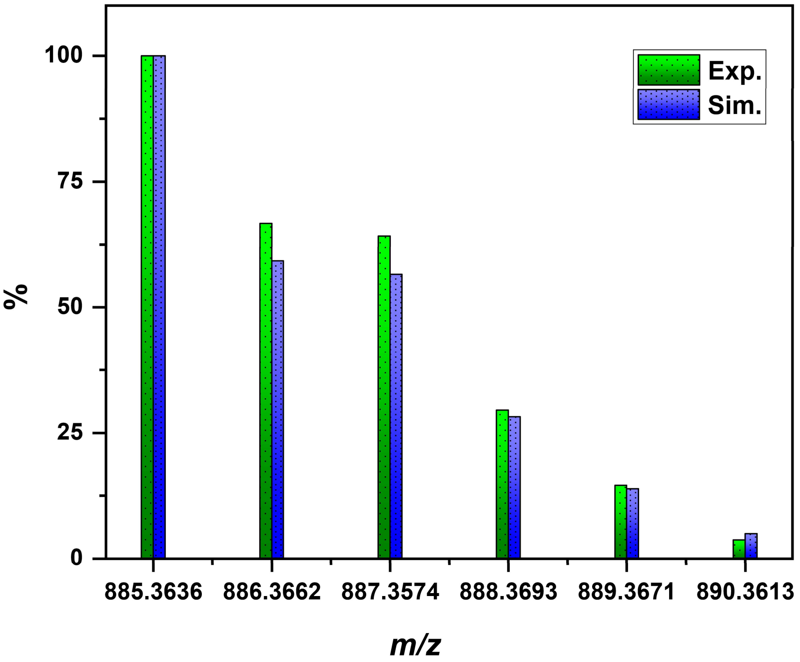

Fig. S10 Positive-Ion ESI-MS spectrum of [Ni(L^{1*})] (**2**): {[Ni(L^{1*})$_2$] + H^+}; *m* / *z* = 885.3636.

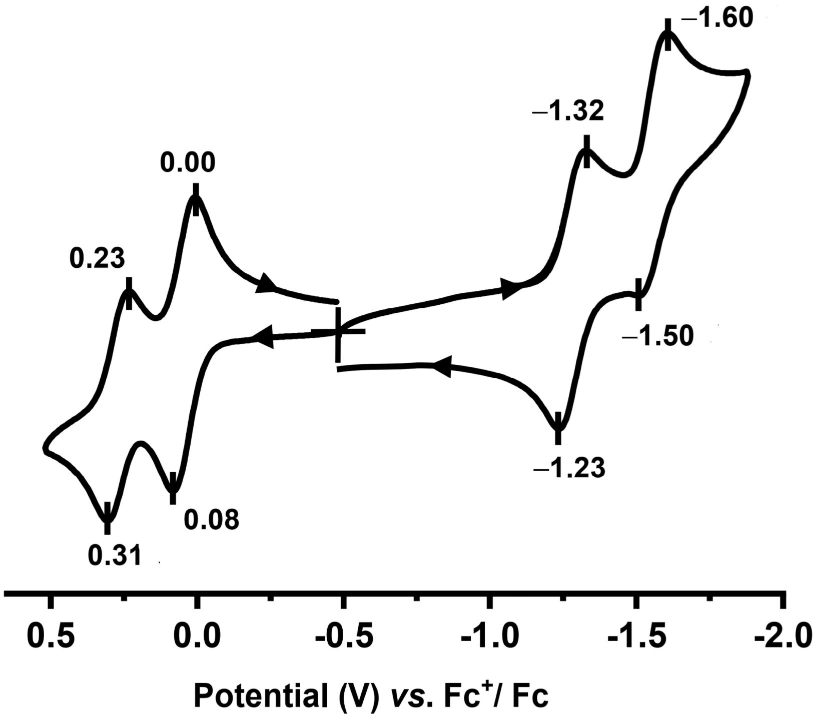

Fig. S11 Cyclic voltammogram of a 1.0 mM solution of **2** in CH_2Cl_2 (0.1 M TBAP; scan rate, 100 mVs^{-1}; Pt working electrode) at 298 K.

Acquisition Parameter

Source Type	ESI	Ion Polarity	Positive	Set Nebulizer	0.4 Bar
Focus	Active	Set Capillary	4500 V	Set Dry Heater	200 °C
Scan Begin	50 m/z	Set End Plate Offset	-500 V	Set Dry Gas	4.0 l/min
Scan End	1000 m/z	Set Charging Voltage	2000 V	Set Divert Valve	Source
		Set Corona	0 nA	Set APCI Heater	0 °C

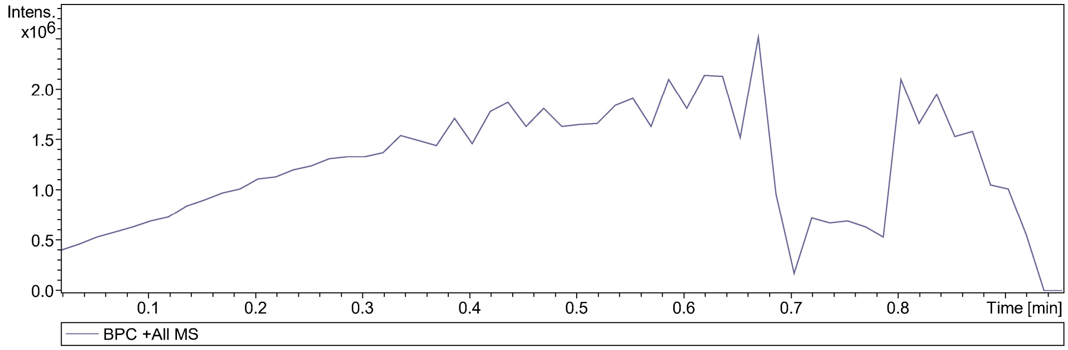

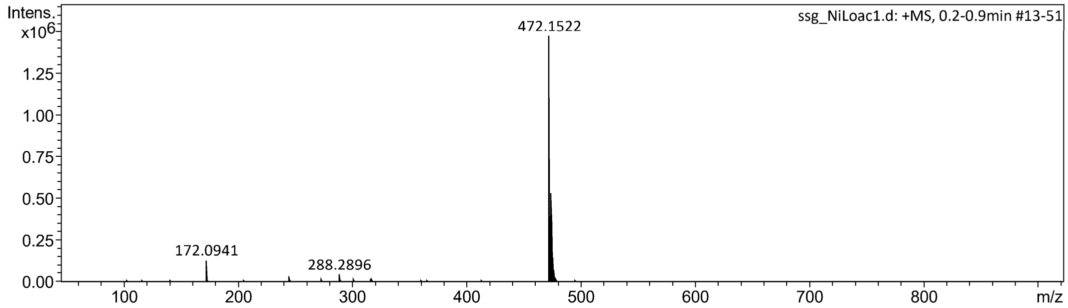

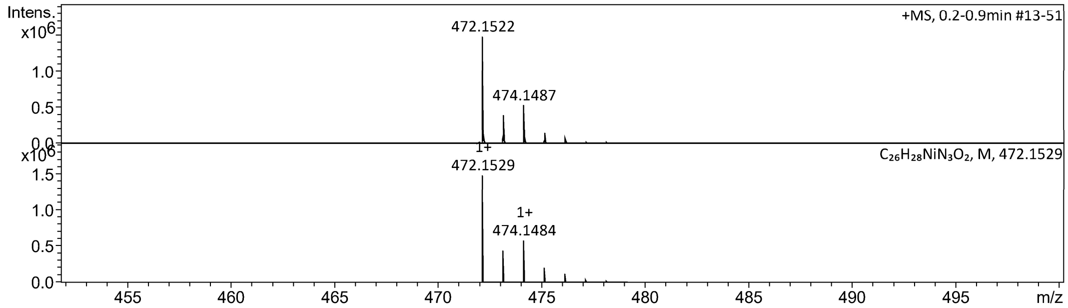

ssg_NiLoac1.d

Bruker Compass DataAnalysis 4.1 printed: 3/5/2024 1:34:20 PM by: IISER Kolkata Page 1 of 1

Fig. S12 Positive-ion ESI-MS analysis of H_3L^1 + Et_3N + $Ni(OAc)_2•4H_2O$ reaction mixture: $\{[Ni(L^1)] - e^-\}^+$; $m\,/\,z$ = 472.1529/472.1522 (calcd/found).

Acquisition Parameter

Source Type	ESI	Ion Polarity	Positive	Set Nebulizer	0.5 Bar
Focus	Active	Set Capillary	3400 V	Set Dry Heater	200 °C
Scan Begin	50 m/z	Set End Plate Offset	-500 V	Set Dry Gas	4.0 l/min
Scan End	3000 m/z	Set Charging Voltage	2000 V	Set Divert Valve	Source
		Set Corona	0 nA	Set APCI Heater	0 °C

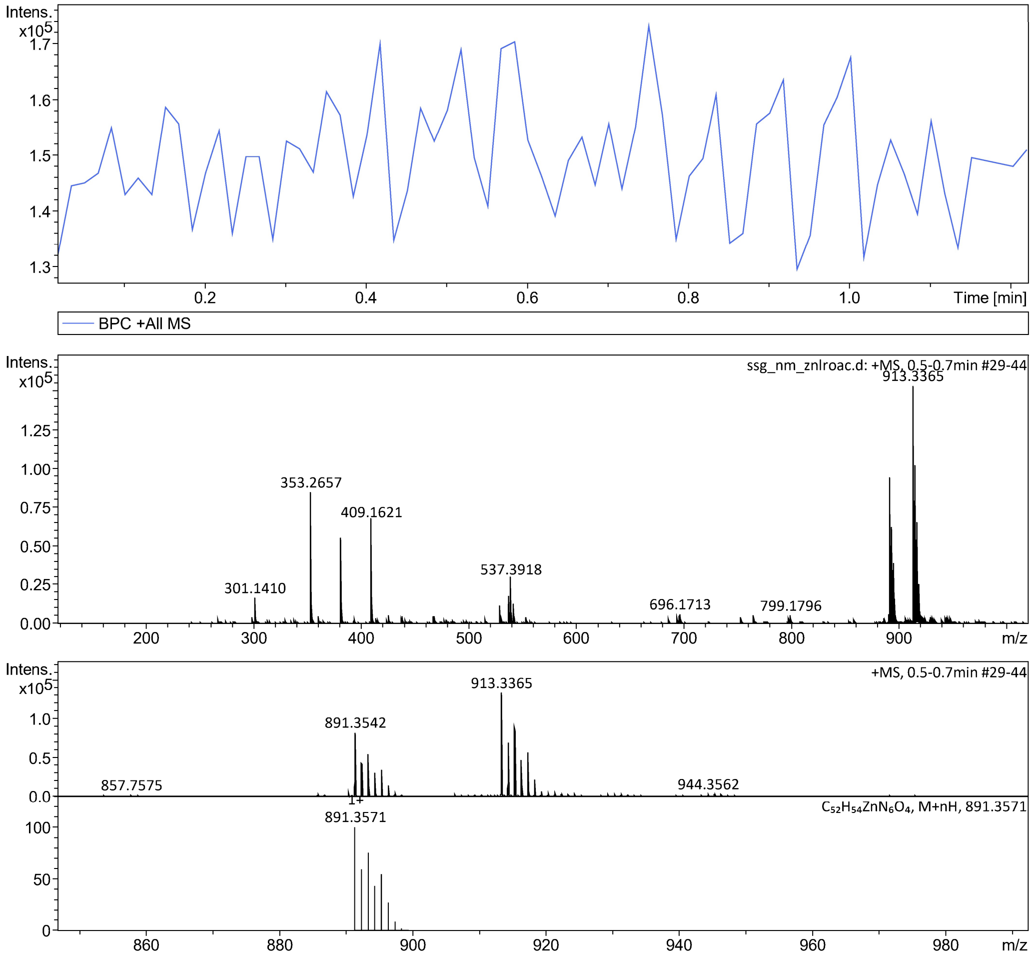

ssg_nm_znlroac.d

Bruker Compass DataAnalysis 4.1 printed: 3/6/2024 3:49:28 PM by: IISER Kolkata Page 1 of 1

Fig. S13 Positive-ion ESI-MS analysis of $HL^{1*}\bullet HClO_4 + Et_3N + Zn(OAc)_2\bullet 2H_2O$ reaction mixture:

$\{[Zn(L^{1*})_2] + H^+\}^+$; $m/z = 891.3571/891.3542$ (calcd/found)

and $\{[Zn(L^{1*})_2] + Na^+\}^+$; $m/z = 913.3396/913.3365$ (calcd/found).

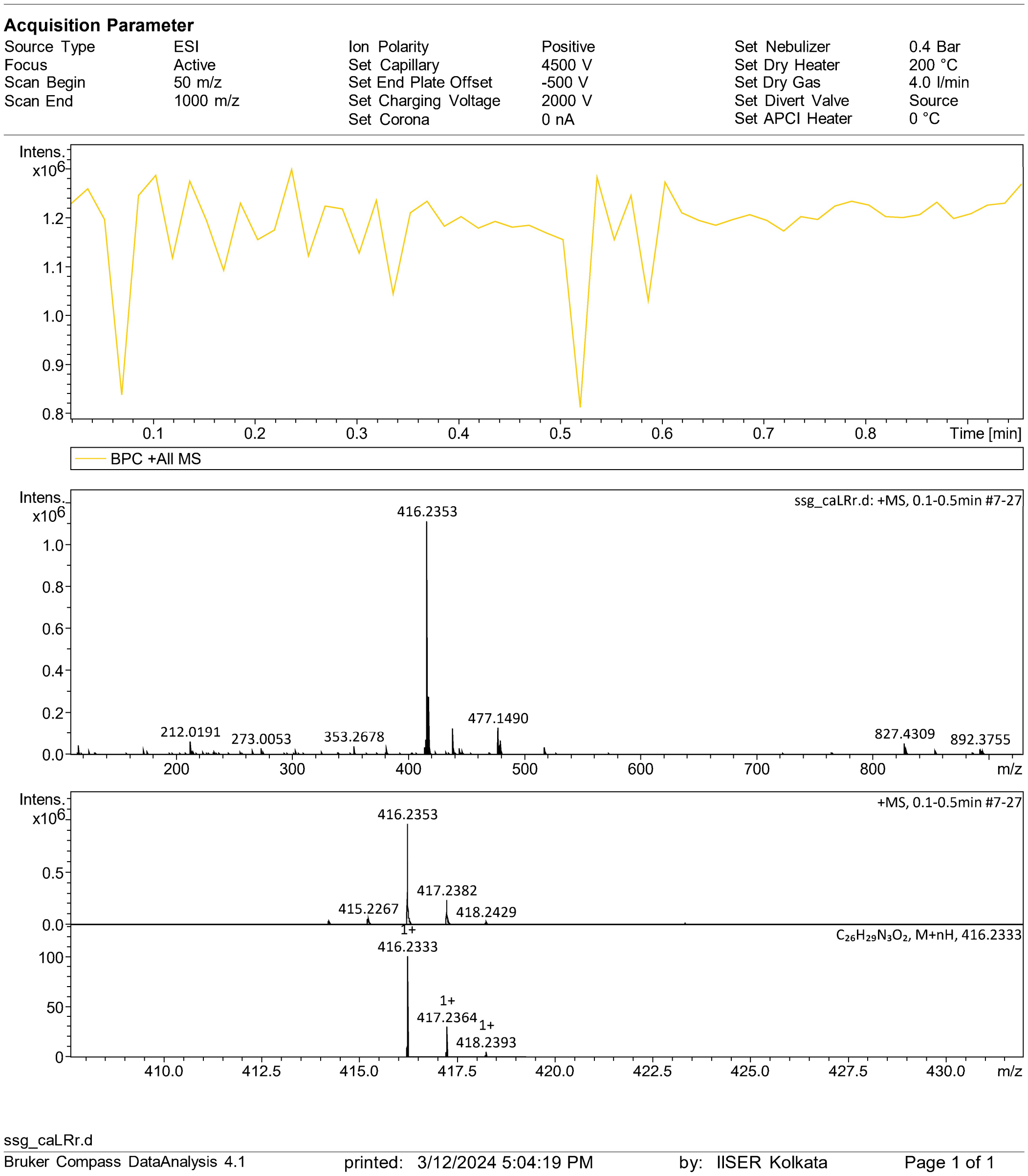

Acquisition Parameter

Source Type	ESI	Ion Polarity	Positive	Set Nebulizer	0.4 Bar
Focus	Active	Set Capillary	4500 V	Set Dry Heater	200 °C
Scan Begin	50 m/z	Set End Plate Offset	-500 V	Set Dry Gas	4.0 l/min
Scan End	1000 m/z	Set Charging Voltage	2000 V	Set Divert Valve	Source
		Set Corona	0 nA	Set APCI Heater	0 °C

ssg_caLRr.d

Bruker Compass DataAnalysis 4.1 printed: 3/12/2024 5:04:19 PM by: IISER Kolkata Page 1 of 1

Fig. S14 Positive-ion ESI-MS analysis of H_3L^1 + Et_3N + $Ca(ClO_4)_2$•xH_2O reaction mixture: $\{H_2L^{1*} + H^+\}^+$; *m / z* = 416.2333/416.2354 (calcd/found).

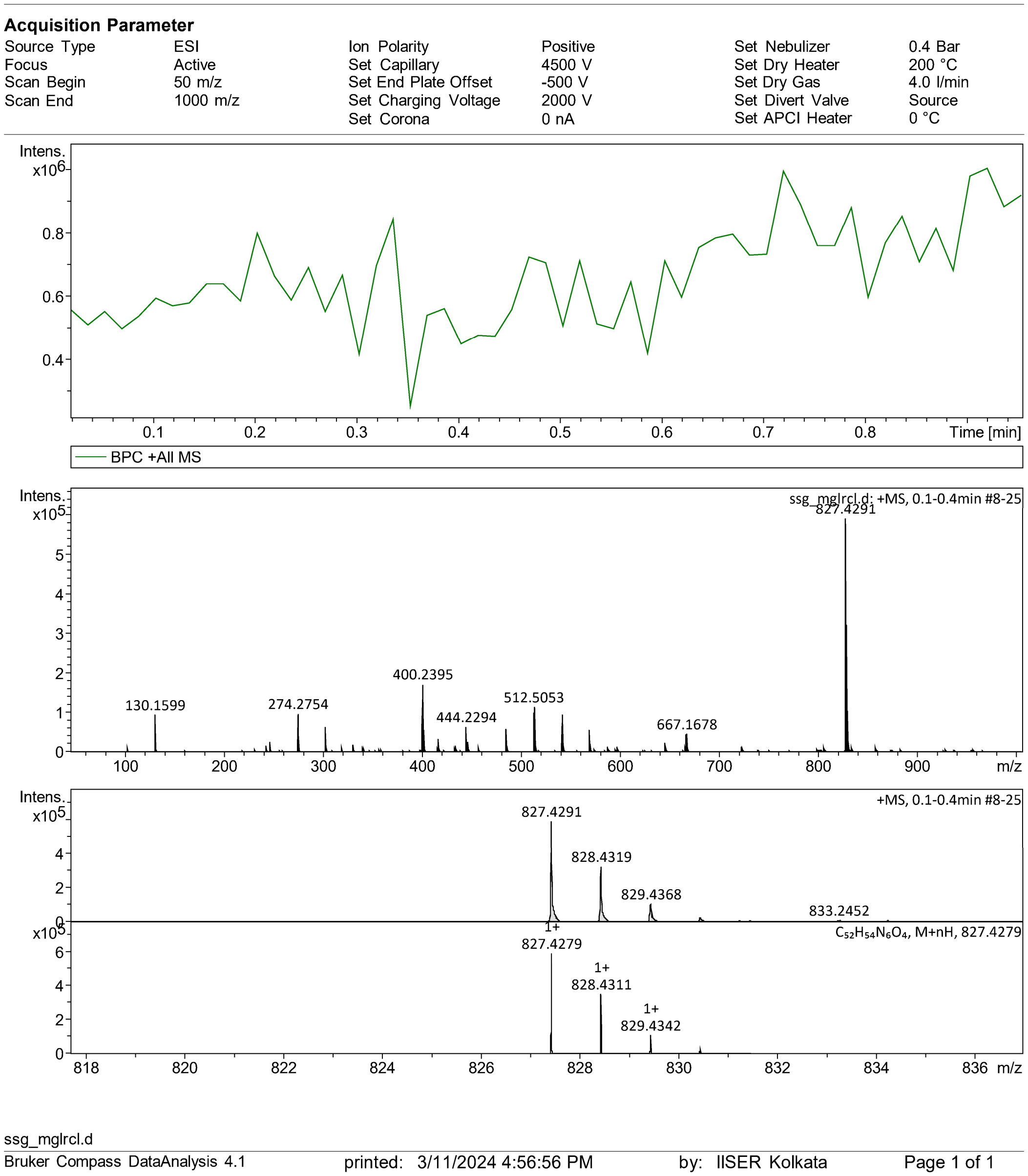

Acquisition Parameter

Source Type	ESI	Ion Polarity	Positive	Set Nebulizer	0.4 Bar
Focus	Active	Set Capillary	4500 V	Set Dry Heater	200 °C
Scan Begin	50 m/z	Set End Plate Offset	-500 V	Set Dry Gas	4.0 l/min
Scan End	1000 m/z	Set Charging Voltage	2000 V	Set Divert Valve	Source
		Set Corona	0 nA	Set APCI Heater	0 °C

ssg_mglrcl.d

Bruker Compass DataAnalysis 4.1 printed: 3/11/2024 4:56:56 PM by: IISER Kolkata Page 1 of 1

Fig. S15 Positive-ion ESI-MS analysis of H_3L^1 + Et_3N + $MgCl_2$ reaction mixture: $\{(L^{1*}\text{-}L^{1*}) + H^+\}^+$; *m / z* = 827.4279/827.4291 (calcd/found).#

#Radical dimerization is probably via oxidative homo-coupling.[4]

Table S1 Data collection and structure refinement parameters for **1**, **PhZ**•0.75CH_2Cl_2 and **2**.

Empirical formula	$C_{52}H_{54}N_6O_4Zn$ (**1**)	$C_{26.75}H_{30.5}Cl_{1.5}F_6N_3O_2Sb$ (**PhZ**•0.75CH_2Cl_2)	$C_{52}H_{54}N_6O_4Ni$ (**2**)
Formula weight	892.38	714.96	885.72
Crystal colour, habit	dark brown, block	dark violet, plate	dark brown, block
Temperature (K)	100(2)	100(2)	100(2)
Wavelength (Å)	0.71073	0.71073	0.71073
Crystal system	Monoclinic	Triclinic	Monoclinic
Space group	*C*2/*c* 1 (no. 15)	*P*-1 (no. 2)	*C*2/*c* (no. 15)
Crystal size (mm^3)	0.3 x 0.2 x 0.2	0.2 x 0.1 x 0.05	0.2 x 0.2 x 0.1
a (Å)	26.7335(16)	16.147(3)	26.392(3)
b (Å)	17.2618(16)	20.413(3)	17.272(3)
c (Å)	23.2287(19)	20.582(4)	23.289(3)
α (°)	90	65.842(3)	90
β (°)	120.956(4)	89.812(5)	120.049(7)
γ (°)	90	81.287(4)	90
V ($Å^3$)	9192.5(13)	6105.4(18)	9189(2)
Z	8	8	8
D_{calc} ($g\ cm^{-3}$)	1.290	1.556	1.280
μ (mm^{-1})	0.587	1.100	0.474
F (000)	3760.0	2868.0	3744.0
no. reflections collected	56195	21549	63664
no. unique reflection	8104 (R_{int} = 0.0687, $R\sigma$ = 0.0432)	21549 (R_{int} = MERG 0, $R\sigma$ = 0.0877)	9399 (R_{int} = 0.0713, $R\sigma$ = 0.0458)
no. reflections used [$I > 2\sigma(I)$]	6292	15999	7230
$R_1{}^a$, $wR_2{}^b$ [$I > 2\sigma(I)$]	$R_1 = 0.0381^a$ $wR_2 = 0.0812^b$	$R_1 = 0.0857^a$ $wR_2 = 0.2164^b$	$R_1 = 0.0383^a$ $wR_2 = 0.0834^b$
$R_1{}^a$, $wR_2{}^b$ (All data)	$R_1 = 0.0606^a$ $wR_2 = 0.0952^b$	$R_1 = 0.1138^a$ $wR_2 = 0.2374^b$	$R_1 = 0.0620^a$ $wR_2 = 0.0980^b$
Goodness-of-fit on F^2	1.069	1.050	1.055

$^aR_1 = \Sigma||F_o| - |F_c||/\Sigma|F_o|$. $^bwR_2 = \{\Sigma[w\,(|F_o|^2 - |F_c|^2)^2]/\ \Sigma[w(|F_o|^2)^2]\}^{1/2}$.

Table S2 Selected bond distances (Å) and bond angles (°) for complex **1**

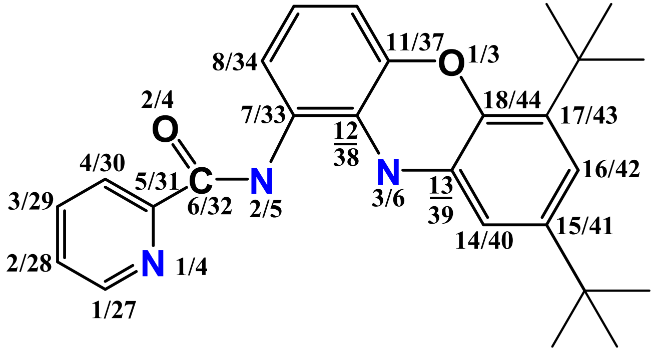

Bond length of 1 in Å at 100 K					
Zn–N1/N4	2.188(2)/ 2.185(2)	Zn–N2/N5	2.086(2)/ 2.068(2)	Zn–N3/N6	2.172(2)/ 2.209(2)
N1–C1/ N4–C27	1.331(3)/ 1.334(3)	C7–N2/ C33–N5	1.384(3)/ 1.384(3)	C12–N3/ C38–N6	1.360(3)/ 1.356(3)
C1–C2/ C27–C28	1.381(4)/ 1.384(3)	C7–C12/ C33–C38	1.443(3)/ 1.442(3)	C13–N3/ C39–N6	1.379(3)/ 1.381(3)
C2–C3/ C28–C29	1.377(4)/ 1.381(4)	C7–C8/ C33–C34	1.398(3)/ 1.396(3)	C13–C14/ C39–C40	1.399(3)/ 1.400(3)
C3–C4/ C29–C30	1.381(4)/ 1.379(4)	C8–C9/ C34–C35	1.396(4)/ 1.389(4)	C14–C15/ C40–C41	1.388(3)/ 1.382(3)
C4–C5/ C30–C31	1.383(4)/ 1.384(3)	C9–C10/ C35–C36	1.383(4)/ 1.388(4)	C15–C16/ C41–C42	1.403(4)/ 1.406(3)
C5–C6/ C31–C32	1.511(4)/ 1.510(3)	C10–C11/ C36–C37	1.374(4)/ 1.377(4)	C16–C17/ C42–C43	1.392(4)/ 1.396(4)
C5–N1/ C31–N4	1.343(3)/ 1.345(3)	C11–O1/ C37–O3	1.373(3)/ 1.377(3)	C17–C18/ C43–C44	1.393(4)/ 1.402(3)
C6–N2/ C32–N5	1.352(3)/ 1.354(3)	C11–C12/ C37–C38	1.406(3)/ 1.409(3)	C18–C13/ C44–C39	1.407(3)/ 1.405(3)
				C18–O1/ C44–O3	1.378(3)/ 1.376(3)

Bond angle of 1 in (°) at 100 K			
N1–Zn–N2	76.55(8)	N2–Zn–N5	168.79(8)
N1–Zn–N3	153.07(8)	N2–Zn–N6	109.28(8)
N1–Zn–N4	98.21(7)	N3–Zn–N4	92.00(7)
N1–Zn–N5	94.19(8)	N3–Zn–N5	112.43(8)
N1–Zn–N6	92.40(7)	N3–Zn–N6	89.77(7)
N2–Zn–N3	77.40(8)	N4–Zn–N5	76.95(8)
N2–Zn–N4	97.88(8)	N4–Zn–N6	152.48(7)
		N5–Zn–N6	77.02(7)

Table S3. TD-DFT-calculated electronic transitions of $[\mathrm{Zn^{II}}\{(\mathrm{L^{1}}{*})^{\bullet-}\}_2]$ (**1**) ($M_\mathrm{S} = 0$).

Excitation energy(eV)	λ (nm)	*f*	Transition	Character
1.73	715	0.0658	α–H−1 [~99%L]→ α–L[~99%L](33%)	CT (amidato part of right ligand → phenoxainyl ring of right ligand)
			β–H−1[~99%L]→ β–L[~99%L](65%)	CT (amidato part of left ligand → phenoxainyl ring of left ligand)
2.60	476	0.0858	α–H[~99%L]→ α–L+1[~99%L](10%)	CT (phenoxazinyl ring of left ligand→ pyridine of left ligand)
			β–H[~99%L]→ β–L+1[~99%L](63%)	CT (phenoxazinyl ring of right ligand→ pyridine of right ligand)
2.80	441	0.0772	α–H−7 [~99%L]→ α–L[~99%L](25%)	π → π* (phenoxazinyl ring of right ligand)
			α–H[~99%L]→ α–L+5[~99%L](18%)	π → π* (phenoxazinyl ring of left ligand)
			β–H−7 [~99%L]→ β–L[~99%L](25%)	π → π* (phenoxazinyl ring of left ligand)
			β–H[~99%L]→ β–L+5[~99%L](18%)	π → π* (phenoxazinyl ring of right ligand)
3.22	385	0.2681	α–H−7 [~99%L]→ α–L[~99%L](19%)	π → π* (phenoxazinyl ring of right ligand)
			α–H[~99%L]→ α–L+5[~99%L](20%)	π → π* (phenoxazinyl ring of left ligand)
			β–H−7 [~99%L]→ β–L[~99%L](20%)	π → π* (phenoxazinyl ring of left ligand)

		β–H[~99%L]→ β–L+5[~99%L](19%)	π → π* (phenoxazinyl ring of right ligand)

Note: No appreciable intensity in the NIR region (1000-2000 nm) can be found from the TD-DFT calculation.

Table S4. DFT-optimized cartesian coordinates of [Zn^{II}(L^{1}*)$_2$] (M_S = 0)

Zn	9.353241000	10.077743000	13.843853000
O	11.804148000	10.861761000	18.166631000
O	8.265318000	14.732969000	12.277354000
O	11.883897000	9.505913000	10.512728000
O	6.201358000	8.191050000	15.926914000
N	8.190772000	9.303763000	15.411009000
N	10.571604000	10.584738000	15.654236000
N	7.513198000	9.267582000	12.799024000
N	8.775313000	12.185331000	13.352549000
N	10.414872000	10.442079000	12.070815000
N	10.529283000	8.166656000	13.518612000
C	7.958308000	13.080575000	14.005612000
C	6.643838000	8.722932000	13.662718000
C	9.995174000	10.075995000	16.774173000
C	5.433585000	8.162641000	13.236100000
H	4.766803000	7.732771000	13.983766000
C	8.726535000	9.380942000	16.679235000
C	9.332149000	12.569970000	12.174642000
C	14.202999000	12.583758000	16.031170000
H	15.149268000	13.107385000	16.118714000
C	7.695642000	14.373432000	13.473967000
C	13.632382000	12.064938000	17.204620000

C	13.622076000	12.465149000	14.751692000
C	7.001832000	8.714561000	15.140125000
C	10.607777000	10.204609000	18.049009000
C	12.405629000	11.392432000	17.051953000
C	7.358027000	12.725121000	15.231405000
H	7.568376000	11.727851000	15.614237000
C	11.215367000	9.479085000	11.554923000
C	10.204751000	11.659960000	11.459092000
C	11.772940000	11.243913000	15.786741000
C	6.043989000	8.745124000	10.982422000
H	5.849004000	8.775786000	9.908749000
C	7.227039000	9.280116000	11.494225000
H	7.976986000	9.734966000	10.841693000
C	8.170828000	8.855760000	17.863986000
H	7.220769000	8.333017000	17.799987000
C	14.284356000	13.053172000	13.488333000
C	5.131333000	8.176236000	11.875057000
H	4.194078000	7.746896000	11.511851000
C	11.270810000	8.218356000	12.402400000
C	9.080057000	13.851531000	11.617085000
C	12.406862000	11.791389000	14.652175000
H	11.907341000	11.659050000	13.694106000
C	8.822673000	9.006204000	19.092693000
H	8.361785000	8.585577000	19.990018000
C	6.529091000	13.609043000	15.918761000
C	5.890511000	13.186860000	17.258553000
C	6.867104000	15.302083000	14.130679000
C	10.555037000	7.067162000	14.277040000
H	9.927028000	7.084422000	15.171731000

C	6.306978000	14.878856000	15.346684000
H	5.663517000	15.574518000	15.875282000
C	14.317952000	12.230011000	18.581196000
C	10.041917000	9.681390000	19.204762000
H	10.553790000	9.805591000	20.160005000
C	10.748418000	12.093682000	10.232527000
H	11.402085000	11.416082000	9.690697000
C	11.333621000	5.954196000	13.955938000
H	11.326041000	5.075759000	14.604039000
C	10.459416000	13.365709000	9.726890000
H	10.899706000	13.667333000	8.773120000
C	15.626113000	13.742682000	13.797618000
H	15.507814000	14.589016000	14.492650000
H	16.058645000	14.141725000	12.866880000
H	16.360974000	13.043910000	14.227703000
C	9.628640000	14.260565000	10.408126000
H	9.401996000	15.255243000	10.021940000
C	13.338130000	14.101386000	12.858712000
H	12.374900000	13.660130000	12.563989000
H	13.793698000	14.534655000	11.953248000
H	13.134036000	14.923185000	13.563899000
C	14.548978000	11.919513000	12.470627000
H	15.217794000	11.154514000	12.896827000
H	15.030229000	12.323602000	11.565097000
H	13.623121000	11.418760000	12.152059000
C	14.644646000	10.842559000	19.185704000
H	13.743292000	10.239538000	19.354156000
H	15.155645000	10.965882000	20.154691000
H	15.316981000	10.276356000	18.521213000

C	13.401295000	13.028627000	19.539546000
H	13.188741000	14.029870000	19.131658000
H	13.900259000	13.161241000	20.513568000
H	12.444043000	12.522014000	19.716872000
C	12.079783000	7.147194000	12.004081000
H	12.659757000	7.246421000	11.086371000
C	5.011316000	14.297318000	17.862539000
H	5.588157000	15.209976000	18.080774000
H	4.577701000	13.948067000	18.812497000
H	4.174452000	14.569281000	17.200020000
C	6.584195000	16.709126000	13.553125000
C	7.007139000	12.853111000	18.274496000
H	7.641114000	12.022063000	17.932580000
H	6.568544000	12.555889000	19.241110000
H	7.656333000	13.726253000	18.449053000
C	7.904760000	17.505023000	13.414785000
H	8.396702000	17.617847000	14.394254000
H	7.695485000	18.514961000	13.025691000
H	8.612827000	17.019982000	12.730722000
C	15.646826000	13.003274000	18.467687000
H	16.376609000	12.485998000	17.825711000
H	16.097353000	13.095932000	19.467912000
H	15.504480000	14.022653000	18.076537000
C	12.110744000	5.999602000	12.795283000
H	12.733704000	5.147738000	12.510754000
C	5.884668000	16.590065000	12.177338000
H	6.506755000	16.068263000	11.438871000
H	5.660007000	17.594247000	11.781822000
H	4.931751000	16.044669000	12.270451000

C	5.005468000	11.938767000	17.036037000
H	4.202303000	12.148564000	16.311302000
H	4.534382000	11.630102000	17.983656000
H	5.581373000	11.079379000	16.662929000
C	5.652544000	17.524611000	14.471679000
H	4.668314000	17.047204000	14.597126000
H	5.481666000	18.516398000	14.025218000
H	6.088441000	17.684771000	15.470002000

Table S5. Computed energy[21] values for $[\mathrm{Zn^{II}}\{(\mathrm{L^{1}}*)^{\bullet-}\}_2]$ (**1**)

Zn	O, N, C, H	Functional	$-E_{\mathrm{HS}}$ (a.u.) $M_s = 1$	$-E_{\mathrm{BS}}$ (a.u.) $M_s = 0$	$\Delta E = -E_{\mathrm{BS}} - (-E_{\mathrm{HS}})$	J_{calc} (in cm^{-1})^{c}
TZVP	SVP	B3LYP	4421.8290358	4421.8290850	−0.031	−7.7 (−27.1)

[a] 1a.u. = 627.50 kcal/mol; 1 kcal/mol = 349.74 cm^{-1}. [b] (ΔE) values in kcal/mol are in parentheses. [c] J_{exp} value is in parentheses. [d] J_{calc} values were calculated using Yamaguchi's approach[17] $[J = -(E_{\mathrm{HS}} - E_{\mathrm{BS}})/(\langle S^2\rangle_{\mathrm{HS}} - \langle S^2\rangle_{\mathrm{BS}})]$ (equation 5).

Table S6. Selected bond distances (Å) and bond angles (°) for **PhZ•**0.75CH_2Cl_2

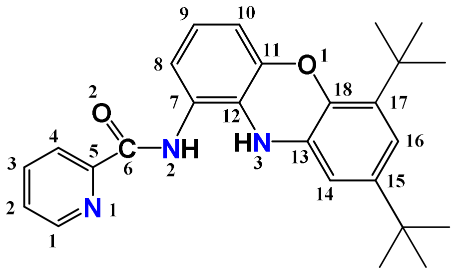

Bond length in Å at 100 K					
N1–C1	1.322(16)	C7–N2	1.381(13)	C12–N3	1.329(13)
C1–C2	1.402(16)	C7–C12	1.439(14)	C13–N3	1.355(13)
C2–C3	1.424(18)	C7–C8	1.374(15)	C13–C14	1.388(15)
C3–C4	1.391(19)	C8–C9	1.384(16)	C14–C15	1.372(15)
C4–C5	1.406(16)	C9–C10	1.374(15)	C15–C16	1.428(16)
C5–C6	1.477(16)	C10–C11	1.420(15)	C16–C17	1.358(17)
C5–N1	1.346(14)	C11–O1	1.336(12)	C17–C18	1.362(14)
C6–N2	1.394(12)	C11–C12	1.413(14)	C18–C13	1.469(14)
				C18–O1	1.331(12)

Table S7 Selected bond distances (Å) and bond angles (°) for complex **$[Ni^{II}(L^{1*})_2^{\bullet-}]$** (**2**).

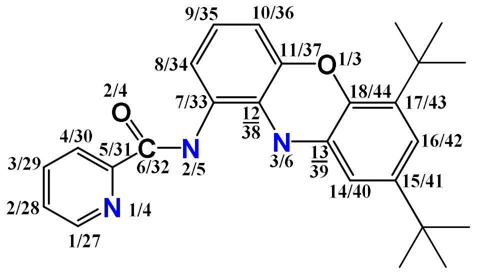

Bond length of 2 in Å at 100 K

Ni–N1/N4	2.117(2)/ 2.120(2)	Ni–N2/N5	2.029(2)/ 2.036(2)	Ni–N3/N6	2.142(2)/ 2.115(2)
N1–C1/ N4–C27	1.334(3)/ 1.340(3)	C7–N2/ C33–N5	1.384(3)/ 1.385(3)	C12–N3/ C38–N6	1.369(3)/ 1.369(3)
C1–C2/ C27–C28	1.383(3)/ 1.376(3)	C7–C12/ C33–C38	1.436(3)/ 1.437(3)	C13–N3/ C39–N6	1.383(3)/ 1.380(3)
C2–C3/ C28–C29	1.382(3)/ 1.389(3)	C7–C8/ C33–C34	1.400(3)/ 1.400(3)	C13–C14/ C39–C40	1.405(3)/ 1.404(3)
C3–C4/ C29–C30	1.382(3)/ 1.386(3)	C8–C9/ C34–C35	1.383(3)/ 1.393(3)	C14–C15/ C40–C41	1.385(3)/ 1.380(3)
C4–C5/ C30–C31	1.386(3)/ 1.387(3)	C9–C10/ C35–C36	1.395(3)/ 1.388(3)	C15–C16/ C41–C42	1.405(3)/ 1.403(3)
C5–C6/ C31–C32	1.507(3)/ 1.512(3)	C10–C11/ C36–C37	1.380(3)/ 1.381(3)	C16–C17/ C42–C43	1.400(3)/ 1.394(3)
C5–N1/ C31–N4	1.356(3)/ 1.350(3)	C11–O1/ C37–O3	1.374(3)/ 1.371(3)	C17–C18/ C43–C44	1.397(3)/ 1.396(3)
C6–N2/ C32–N5	1.350(3)/ 1.350(3)	C11–C12/ C37–C38	1.406(3)/ 1.405(3)	C18–C13/ C44–C39	1.404(3)/ 1.410(3)
				C18–O1/ C44–O3	1.387(2)/ 1.379(3)

Bond angle of 2 in (°) at 100 K			
N1–Ni–N2	78.36(7)	N2–Ni–N5	168.64(7)
N1–Ni–N3	156.12(7)	N2–Ni–N6	110.35(7)
N1–Ni–N4	95.82(7)	N3–Ni–N4	91.73(7)
N1–Ni–N5	95.34(7)	N3–Ni–N5	108.38(7)
N1–Ni–N6	92.14(7)	N3–Ni–N6	89.82(7)
N2–Ni–N3	78.65(7)	N4–Ni–N5	78.18(7)
N2–Ni–N4	92.94(7)	N4–Ni–N6	156.48(7)
		N5–Ni–N6	79.08(7)

Scheme S1 Plausible mechanism for the formation of $\{\mathbf{L^{1*}}\}^{\bullet-}$ in complex **1** (metal coordination is omitted for clarity)